

## Clinical Feasibility of Microscopically-Guided Breast Needle Biopsy Using a Fiber-Optic Probe with Computer-Aided Detection

www.tcrt.org

Needle biopsy of small or nonpalpable breast lesions has a high nondiagnostic sampling rate even when needle position is guided by stereotaxis or ultrasound. We assess the feasibility of using a near-infrared fiber optic probe and computer-aided detection for the microscopic guidance of needle breast biopsy procedures. Specimens from nine consented patients undergoing breast-conserving surgery were assessed intraoperatively using a needle device with an integrated fiber-optic probe capable of assessing two physical tissue properties highly correlated to pathology. Immediately following surgical resection, specimens were probed by inserting the optical biopsy needle device into the tissue, simulating the procedure used to position standard biopsy needles. Needle positions were marked and correlated with histology, which verified measurements obtained from 58 needle positions, including 40 in adipose and 18 in tumor tissue. This study yielded tissue classifications based on measurement of optical refractive index and scattering. Confidence-rating schemes yielded combined sensitivity of 89% (16/18) and specificity of 78% (31/40). Refractive index tests alone identified tumor tissue with a sensitivity of 83% (15/18) and specificity of 75% (30/40). Scattering profiles independently identified tumor tissue with a sensitivity of 61% (11/18) and specificity of 60% (24/40). These results show that a biopsy needle with an integrated fiber optic probe can be used to identify breast tumor tissue for sampling. Integration of this probe into current practices offers the potential to reduce nondiagnostic sampling rates by directly evaluating *in situ* microscopic tissue properties in real-time, before removal.

Key words: Biopsy Guidance; Breast Cancer; Computer-Aided Detection; Optical Coherence Tomography.

### Introduction

Needle biopsy of breast masses is widely recognized as a highly accurate and economical diagnostic procedure when tissue sampling is sufficient. However, core-needle biopsy (CNB) and fine-needle aspiration biopsy (FNAB) procedures both suffer from significant nondiagnostic sampling rates when in the hands of inexperienced operators (1-4) or, in the case of CNB, when small or non-palpable masses are targeted (5-8). Nondiagnostic samples, typically classified as those which are void of epithelial cells (4), occur in up to 35% of palpation-guided FNAB (1-3) procedures and 12% of image-guided CNB procedures targeting nonpalpable lesions (9). These difficulties lead to rebiopsy in approximately 4% of the patients that undergo percutaneous procedures (10-11).

Adam M. Zysk, Ph.D.<sup>1</sup>  
Freddy T. Nguyen, B.S.<sup>2</sup>  
Eric J. Chaney, B.S.<sup>1</sup>  
Jan G. Kotynek, M.D.<sup>4</sup>  
Uretz J. Oliphant, M.D.<sup>4</sup>  
Frank J. Bellafiore, M.D.<sup>4</sup>  
Patricia A. Johnson, M.D., Ph.D.<sup>4</sup>  
Kendrith M. Rowland, M.D.<sup>4</sup>  
Stephen A. Boppart, M.D., Ph.D.<sup>1,3,4\*</sup>

<sup>1</sup>Department of Electrical and  
Computer Engineering

<sup>2</sup>Department of Chemistry  
Medical Scholars Program  
College of Medicine

<sup>3</sup>Department of Electrical and  
Computer Engineering

<sup>1,2,3</sup>Beckman Institute for Advanced  
Science and Technology  
Department of Bioengineering  
College of Medicine,  
University of Illinois at Urbana-  
Champaign

<sup>4</sup>Mills Breast Cancer Institute  
Carle Foundation Hospital  
Carle Clinic Association.

\*Corresponding Author:  
Stephen A. Boppart, M.D., Ph.D.  
Email: boppart@illinois.edu

**Abbreviations:** CNB, Core Needle Biopsy; FNAB, Fine Needle Aspiration Biopsy; H&E, Hematoxylin and Eosin; OCT, Optical Coherence Tomography.

Integrated sensing systems are not currently used for needle guidance. Rather, palpation or external imaging, commonly x-ray stereotaxis or ultrasound imaging, are used. These imaging techniques are typically time consuming, are expensive, and require additional staff and expert operators (12). Also, the diagnostic accuracy of ultrasound-guided biopsy has been questioned in the literature (9, 13-14). Additionally, with the increasing use of more sensitive screening techniques, such as digital mammography and breast MRI, the number of needle biopsy procedures performed on small nonpalpable lesions is likely to rise. These issues have led to increasing interest in point-of-biopsy imaging systems that can assess the tissue at the needle tip prior to removal (15-17).

In this work, we have studied the application of a fiber-optic imaging device and associated computer-aided detection techniques to this problem. We have applied the techniques of optical coherence tomography (OCT), an established optical imaging technique that can provide real-time cross-sectional images of tissue morphology, to the intraoperative study of breast biopsy guidance. The OCT technique is analogous to ultrasound imaging. It is used to measure subsurface reflections of near-infrared light and provides cross-sectional image detail on the scale of conventional histology. It has been successfully applied to a number of clinical problems and is best known in ophthalmology, where it is used to image the retina in cross-section (18). The application of OCT to breast imaging is a rapidly emerging area of interest that has

seen advances in surgical margin detection, lymph node evaluation, and computer-aided diagnostics (16, 19-25).

The system used in this study measured both the optical refractive index and the optical scattering response of the tissue through the needle tip. Refractive index is an established diagnostic property that is regularly incorporated into clinical measurements to assess and identify tissues of interest, for example in blood oxygenation sensors (26). Refractive index is linked to the chemical state of tissue, specifically the protein density and lipid concentrations. Recent studies showed that it is an effective means by which to differentiate between fibrofatty and epithelial mammary tissues (27) and potentially between lesion pathology (28). In addition to refractive index, the tissue scattering signature, the key means of OCT image formation, holds significant diagnostic information about the structure and morphology of the tissue, as has been demonstrated in multiple breast imaging studies (16,19-25). The work presented here is the first reported intraoperative study of these combined techniques for the guidance of breast needle biopsy.

#### Materials and Methods

Ten patients undergoing breast-conserving surgery were recruited into this study under an IRB-approved protocol (see Table 1 for patient and specimen information). Informed consent was obtained prior to each surgery, during which specimens were excised according to the standard of care. After excision, each specimen was immediately transferred to the research staff in the operating room, where it was analyzed with the needle imaging device. The device, which was marked for depth correlation, was inserted by hand to three depths (0.5 mm, 1.0 mm, and 1.5 mm) at three lateral positions approximately 2.0 mm apart along a line (Figure 1). The probe was held in place for several seconds at each position while 1,000 axial optical depth-scans were acquired. The relevant tissue region was subsequently labeled with ink for later correlation with histology, and the specimen was returned to the surgical staff for standard specimen processing procedures, which often included radiological evaluation of the margin status. Along with standard processing, a histology section was taken in the analysis plane to provide correlation to the optical needle data. H&E stained histology of the tissues, with the needle tip positions marked, are shown in Figure 2. Note that the results from one patient were eliminated from the study because the

**Table 1**

Ten patients undergoing breast-conserving surgery were enrolled in the study. The patient age, specimen dimensions, and diagnosis from pathology are shown here. Tumor size information marked with "N/A" was not available upon gross examination. Letters in the first column correspond to the histology images in Figure 2.

	Patient Age	Tumor Size (greatest dimension)	Specimen Size (greatest dimension)	Diagnosis
a	63	N/A	8.0 cm	ductal carcinoma <i>in situ</i>
b	80	N/A	9.0 cm	ductal carcinoma <i>in situ</i>
c	66	1.7 cm	8.5 cm	invasive ductal carcinoma
d	55	1.3 cm	7.1 cm	invasive carcinoma (ductal and predominantly lobular features)
e	40	0.15 cm	5.8 cm	tubular carcinoma and ductal carcinoma <i>in situ</i>
f	73	2.2 cm	6.8 cm	invasive ductal carcinoma
g	79	N/A	6.0 cm	ductal carcinoma <i>in situ</i>
h	43	1.9 cm	7.0 cm	invasive ductal carcinoma
i	42	1.6 cm	5.0 cm	ductal carcinoma <i>in situ</i>
*	57*	0.9 cm*	6.5 cm*	ductal carcinoma <i>in situ</i> *

\*Note that results from the final patient were eliminated from the study (see text).

histology was in stark disagreement with gross intraoperative observations; a handling or labeling error is suspected to have occurred. All hospital staff and physicians were blinded to the results of the study at all stages.

Optical and computer instruments were integrated into a standard endoscopy instrument cart that was wheeled into the operating room for each procedure (Figure 3a). The spectral-domain OCT instrument (Figure 3c) consisted of a near-infrared superluminescent diode light source (Model SLD1C; B&W Tek, Newark, Delaware;  $\lambda_0=1310$  nm,  $\Delta\lambda=92$  nm,  $P=10$  mW) coupled to a fiber-optic interferometer that captured reflection data from the needle apparatus with a high-speed camera (SU1024LE-1.7T1-0500; Sensors Unlimited, Princeton, New Jersey) capable of acquiring 5,000 axial scans per second. The data were acquired and stored on an integrated personal computer that also included a graphical control interface. The low power and near-infrared optical wavelengths used in OCT systems ensure that tissue heating is undetectable; tissue damage due to this low-light exposure has never been reported. The OCT system used in this study is configured to acquire real-time data to a depth of 1-2 mm at an axial resolution of 5.9  $\mu\text{m}$  in tissue, and with a measured signal-to-noise ratio of over 100 dB.

The needle probe device (Figure 3b) was designed to be integrated into a Boston Scientific EasyCore 20G core biopsy device. It is intended to be used with the guide sheath and in place of the cutting needle. The device was constructed from 20 gauge stainless-steel hypodermic tubing which was angled at the tip (36.6 degrees) for cutting during insertion

and for appropriate optical reflection characteristics. The optical components, consisting of an optical fiber (SMF28) and a fiber-optic focusing component (GIF625, Thorlabs, New Jersey), were mounted into the needle with rigid optical cement that formed a flat surface at the tissue-needle interface. Full device specifications and a description of the optical methods used to measure tissue scattering and refractive index characteristics are described in detail elsewhere (29). Briefly, the optical scattering response from within the tissue was measured over a single scan line as is typical in an axial-mode OCT technique. Reflection refractometry was employed by using known properties of the probe tip and a measure of the reflection intensity at the probe-tissue interface to calculate the tissue refractive index based on Fresnel refraction relations. Confounding reflection intensity variations due to movement of the probe fiber were obviated by randomizing the polarization of the input light and averaging over the scan line data taken at each probe position.

Figures 4a and 4b show representative scattering responses from adipose and tumor tissues. The adipose tissue is characterized by discrete peaks representing the boundaries and membranes within the adipose tissue with wide spacing between scattering events and gradual attenuation. In contrast, the tumor tissue has few discrete peaks with little spacing between scattering structures and rapid attenuation, which indicate dense tissue with high nuclear-to-cytoplasmic ratio.

Computer analysis was performed on the acquired data. The refractive index data were used to differentiate between epithelial structures, including tumor, and adipose tissue due to the difference in lipid concentration. Previously published data were used to set a threshold refractive index value for classification. The threshold was set at the midpoint  $n_{\text{threshold}}=1.428$ , between the published values (27) of  $\text{mean}(n_{\text{epithelial}})=1.389$  and  $\text{mean}(n_{\text{adipose}})=1.467$ . Refractive index values above the threshold were classified as adipose and those below as epithelial tissue. Acquired scattering signatures were processed for differentiation between tumor, epithelial stroma, and adipose tissues using computational methods described in detail elsewhere (24). Briefly, the weighted spatial frequency signature of each axial scan (examples shown in Figures 4c and 4d) was compared to the signatures from a training data set from known tissues. The most similar training data, as computed by finding the minimum error, yielded the classification. In this case, since previous intraoperative clinical data is not available, an established "leave-one-out" self-training scheme was used, wherein each data point is compared to

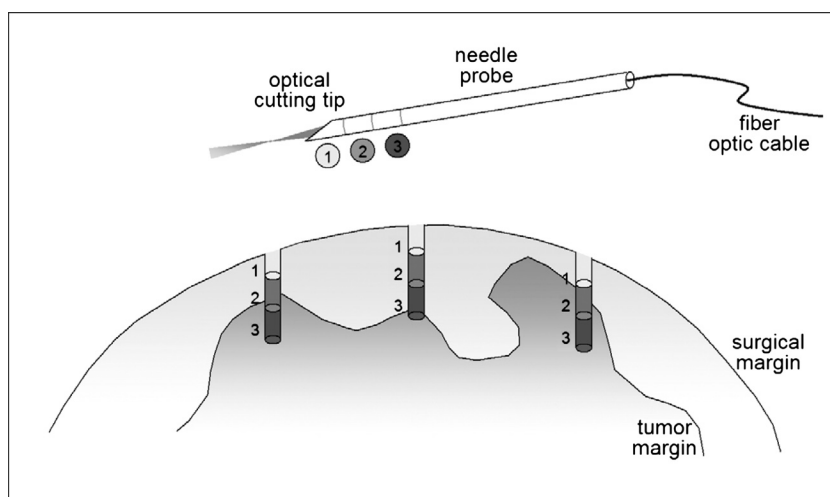


**Figure 1:** Illustration of the data acquisition protocol. A fiber-optic needle probe, marked for three insertion depths (labeled 1, 2, 3), was inserted into excised specimens at three lateral positions. The regions were marked with India ink for correlation with histology prior to standard processing.

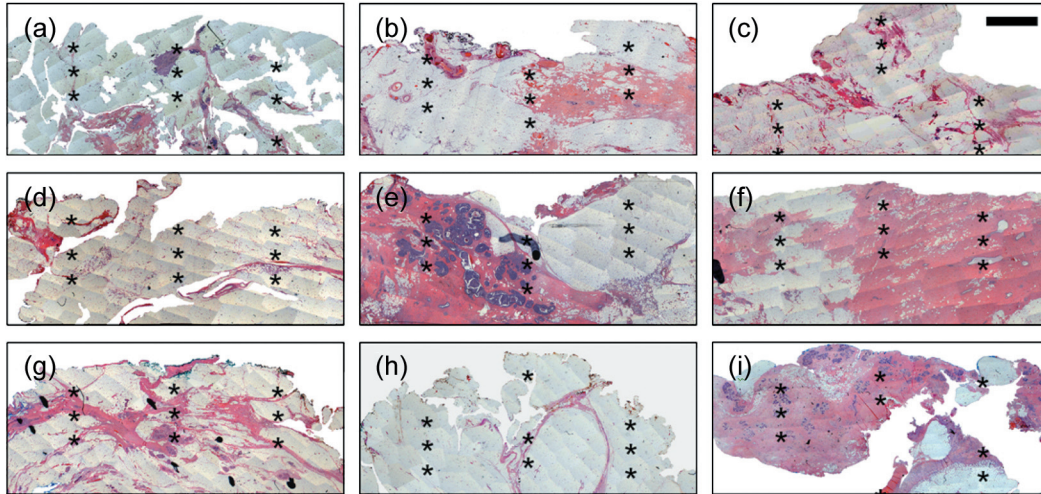


**Figure 2:** Corresponding histology for patient data in Table I. A histologic section from each specimen was cut from the marked region and H&E stained by the pathology department. The resulting slides are shown here for each patient. Needle tip probing positions are marked by asterisks. The scale bar is 1 mm in length. Images were formed by combining multiple high-magnification images using commercial software.

all of the other histology-verified data in the study, which are defined as the training data.

### Results

Intraoperative needle positions were correlated with histology, yielding data from 40 regions of adipose and 18 regions of tumor tissue. In order to perform statistical analysis of the

results, regions containing a mix of tissue types, defined as less than 85% of a single tissue type, were excluded from the data set. Identification of tumor tissue based on refractive index measurements alone had a sensitivity of 83.3% (15/18), a specificity of 75.0% (30/40), and an accuracy of 77.6% (45/58). Among tissue regions classified as tumor, the mean refractive index was  $n_{tumor} = 1.405$ , and among those classified as adipose the mean was  $n_{adipose} = 1.451$ . These values follow the trend of previously published values and hence contribute to the overall confidence in experimental methodology. Tumor tissue identification from the scattering profile alone had a sensitivity of 61.1% (11/18), a specificity of 60.0% (24/40), and a diagnostic accuracy of 60.3% (35/58).

Although the results from scattering measurements alone are not impressive, they can be used in combination with the refractive index classification. This can be accomplished in a number of ways. Standard combination techniques can be used to enhance sensitivity to  $\text{sensitivity}_{\text{refractive index}} + \text{sensitivity}_{\text{scattering}} - (\text{sensitivity}_{\text{refractive index}} \times \text{sensitivity}_{\text{scattering}}) = 90.0\%$  at the expense of specificity, or to boost specificity to  $1 - [(1 - \text{specificity}_{\text{refractive index}}) \times (1 - \text{specificity}_{\text{scattering}})] = 93.5\%$  at the expense of sensitivity (30). Alternatively, specialized methods can be used to assign confidence weights to each method-specific classification ( $c_{ri}$  and  $c_{scatter}$ ). This technique is described in detail elsewhere (24). Briefly, in the case of refractive index measurement, the difference between the measured and threshold refractive index  $\Delta n = |n_{\text{threshold}} - n_{\text{measured}}|$  was

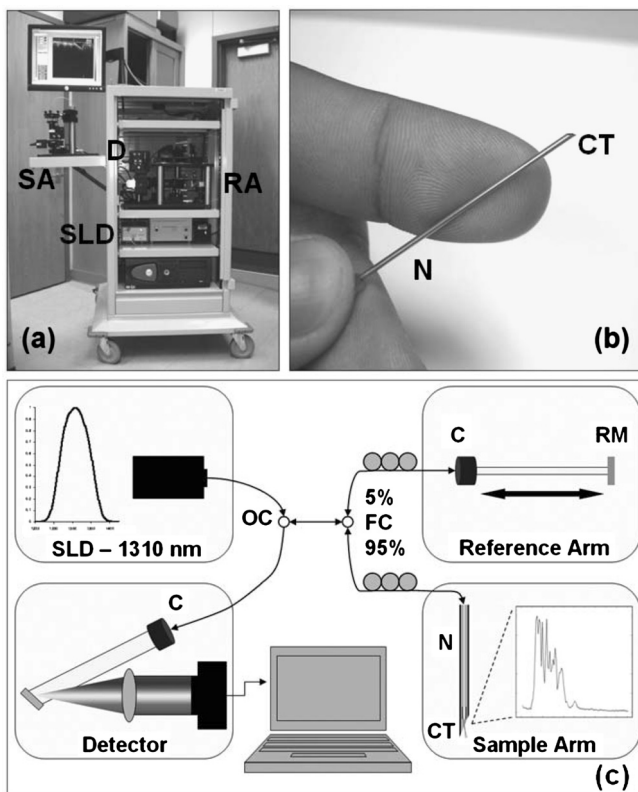


**Figure 3:** The clinical OCT system and needle device used to acquire data. The system is housed in an endoscopy equipment cart (a). The handheld probe (b) is coupled to the Fourier-domain OCT system (c) with a fiber-optic cable. (C – collimator, CT – needle cutting tip, D – detector, FC – fiber coupler/collimator, N – needle housing, OC – optical circulator, RA – reference arm, RM – reference mirror, SA – sample arm, SLD – superluminescent diode).

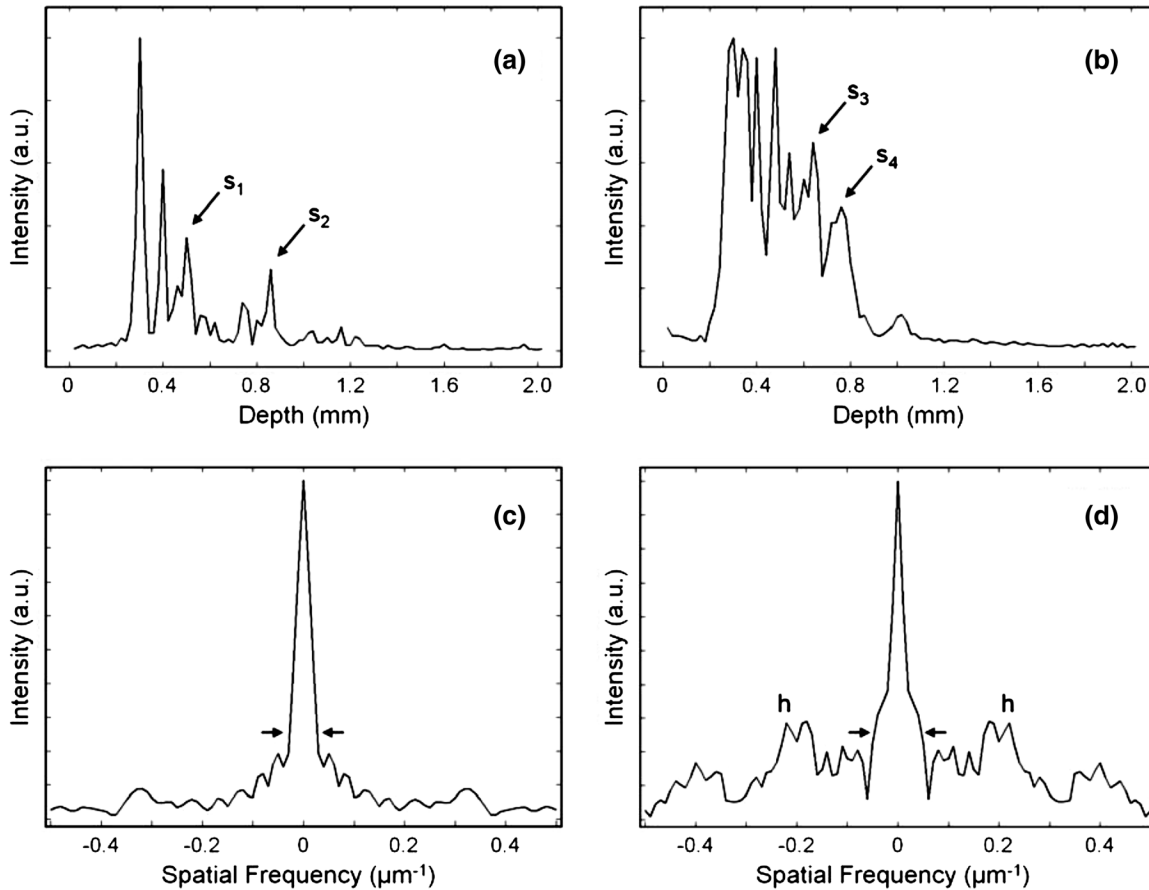


**Figure 4:** Axial-scan scattering responses from the needle device (intensity data scaled for display purposes). Data are shown from fatty tissue (a) and tumor tissue (b). Note that the scattering events have a wider spacing in the fatty tissue (between peaks  $s_1$  and  $s_2$ , for example) due to the large adipocytes cell size when compared to the small dense cells in tumor tissue (note the spacing between  $s_3$  and  $s_4$ , for instance). The spatial frequency components from adipose (c) and from tumor (d) tissues show significantly different signatures as well. The wider central peak (arrows) and prominent high-frequency components (h) are evident for tumor tissue. These features are used to classify the acquired data.

normalized to arrive at a classification confidence value  $c_{fi} = \Delta n / \Delta n_{\max}$ , where  $\Delta n_{\max}$  is the maximum value over all patients in the data set. In the case of scattering measurements, the computed error between the measurement and the training data, which takes values from zero to one, was used as the classification confidence value  $c_{\text{scatter}}$ . In instances of disagreement between the two measurement types, the result with the largest confidence value was used. This method yielded a combined sensitivity of 88.9% (16/18), a specificity of 77.5% (31/40), and an accuracy of 81.0% (47/58).

### Discussion

Previous *in situ* laboratory-based classification studies using these computational techniques yielded sensitivity and specificity measurements of up to 99% and 68%, respectively. There are numerous sources of error that may contribute to this discrepancy. One is the difference between the instruments used in the studies, with the laboratory study employing a free-space imaging geometry as opposed to a handheld probe. Another is the fact that the laboratory work studied

only invasive ductal carcinoma lesions, while this study has analyzed many lesion types. Perhaps most significant is the uncertainty introduced *via* the histology correlation in this study. While significant efforts were made to co-register the needle tip placement with the subsequent sectioning, it is probable that some limited error occurred in this process. The tissue region probed was marked on the surface with a pair of lines indicating the region to be sectioned and the probe was inserted perpendicular to the tissue surface. However, the effects of compression for radiologic assessment and of histologic processing are well known to lead to physical distortions that could affect the sectioning plane location and, hence, the tissue registration. Despite these factors, the results here compare well with established clinical techniques. The sensitivity of ultrasound and x-ray mammography to the detection of invasive ductal carcinoma are 94% and 81%, respectively, when radiologist readers are employed (31). It should be noted that these modalities are sensitive to macroscopic features as opposed to the cellular-scale morphology and composition probed by the techniques presented here. Indeed, it is the ability to identify these small-scale features that

distinguishes this technique and makes it ideal for microscopic positioning of biopsy needles.

The computer-aided detection of these data was performed after the intraoperative acquisition, but real-time analysis is possible with simple system upgrades. A standard personal computer (3.2 GHz Pentium® D processor, 2.0 GB RAM) can analyze the axial-scan data at a rate of over 60 axial scans per second. This processing rate, combined with the speed of the OCT imaging system, which can acquire 5,000 axial scans per second, makes real-time tissue analysis with this device a straightforward prospect.

We have demonstrated that a needle device with an integrated fiber optic probe and associated computer-aided detection algorithms can be used to accurately identify breast lesions under intraoperative protocols that mimic the guidance of needle biopsies. The device is designed to be easily integrated into a commercial 20 gauge core needle biopsy device for clinical use. Integration of this probe into breast biopsy procedures promises to reduce non-diagnostic sampling rates by sensing the microscopic properties of the *in situ* tissue before removal.

#### Acknowledgements

We thank Ann Benefiel, Mary Collins, Barbara Hall, and the research support staff at Carle Foundation Hospital and Carle Clinic Association for their assistance in coordinating the clinical aspects of this study. This research was supported by grants from Carle Foundation Hospital, Urbana, Illinois, the National Institutes of Health (Roadmap Initiative and NIBIB, 1 R21 EB005321 and 1 R01 EB005221, S.A.B.), and the Grainger Foundation (S.A.B.).

#### References

- Boerner, S., Sneige, N. Specimen adequacy and false-negative diagnosis rate in fine-needle aspirates of palpable breast masses. *Cancer* 84, 344-348 (1998).
- Hindle, W. H., Chen, E. C. Accuracy of mammographic appearances after breast fine-needle aspiration. *Am J Obstet Gynecol* 176, 1286-1290 (1997).
- Saxe, A., Phillips, E., Orfanou, P., Husain, M. Role of sample adequacy in fine needle aspiration biopsy of palpable breast lesions. *Am J Surg* 182, 369-371 (2001).
- Ljung, B. M., Drejet, A., Chiampì, N., Jeffrey, J., Goodson, W. H., Chew, K., Moore, D. H., Miller, T. R. Diagnostic accuracy of fine-needle aspiration biopsy is determined by physician training in sampling technique. *Cancer* 93, 263-268 (2001).
- Acheson, M. B., Patton, R. G., Howisey, R. L., Lane, R. F., Morgan, A. Histologic correlation of image-guided core biopsy with excisional biopsy of nonpalpable breast lesions. *Arch Surg* 132, 815-818 (1997).
- Vega Bolivar, A., Ortega García, E., Garijo Ayensa, F. Stereotaxic core needle aspiration biopsy with multiple passes in nonpalpable breast lesions. *Acta Radiol* 39, 389-394 (1998).
- Lieberman, L., Ernberg, L. A., Heerd, A., Zakowski, M. F., Morris, E. A., LaTrenta, L. R., Abramson, A. F., Dershaw, D. D. Palpable breast masses: is there a role for percutaneous imaging-guided core biopsy? *Am J Roentgenol* 175, 779-787 (2000).
- Pijnappel, R. M., van Dalen, A., Borel Rinkes, I. H. M., van den Tweel, J. G., Mali, W. P. T. M. The diagnostic accuracy of core biopsy in palpable and non-palpable breast lesions. *Eur J Radiol* 24, 120-123 (1997).
- Pijnappel, R. M., van den Donk, M., Holland, R., Mali, W. P. T. M., Peterse, J. L., Hendriks, J. H. C. L., Peeters, P. H. M. Diagnostic accuracy for different strategies of image-guided breast intervention in cases of nonpalpable breast lesions. *Br J Cancer* 9, 595-600 (2004).
- Wiratkapun, C., Wibulpholprasert, B., Wongwaisayawan, S., Pulpinyo, K. Nondiagnostic core needle biopsy of the breast under imaging guidance: result of rebiopsy. *J Med Assoc Thai* 88, 350-357 (2005).
- Dershaw, D. D., Morris, E. A., Liberman, L., Abramson, A. F. Nondiagnostic stereotaxic core breast biopsy: results of rebiopsy. *Radiology* 198, 323-325 (1996).
- Azavedo, E., Svane, G., Auer, G. Stereotactic fine-needle biopsy in 2594 mammographically detected non-palpable lesions. *Lancet* 1, 1033-1036 (1989).
- Lieberman, L., Feng, T. L., Dershaw, D. D., Morris, E. A., Abramson, A. F. US-guided core breast biopsy: use and cost-effectiveness. *Radiology* 208, 717-723 (1998).
- Parker, S. H., Jobe, W. E., Dennis, M. A., Stavros, A. T., Johnson, K. K., Yakes, W. F., Truell, J. E., Price, J. G., Kortz, A. B., Clark, D. G. US-guided automated large-core breast biopsy. *Radiology* 187, 507-511 (1993).
- Zhu, C., Palmer, G. M., Breslin, T. M., Xu, F., Ramanujam, N. Use of a multiseparation fiber optic probe for the optical diagnosis of breast cancer. *J Biomed Opt* 10, 024032 (2005).
- Goldberg, B. D., Ifitimia, N. V., Bressner, J. E., Pitman, M. B., Halpern, E., Bouma, B. E., Tearney, G. J. Automated algorithm for differentiation of human breast tissue using low coherence interferometry for fine needle aspiration biopsy guidance. *J Biomed Opt* 13, 014014 (2008).
- Shakhova, N., Turchin, I., Kamensky, V., Sergeeva, E., Golubyatnikov, G., Da Silva, L., Kasthuri, U., Pavlycheva, I., Smetanina, S., Artifeksova, A. Novel optical spectroscopy system for breast cancer diagnostics. *Proceedings of the SPIE* 6430, 64300N (2007).
- Zysk, A. M., Nguyen, F. T., Oldenburg, A. L., Marks, D. L., Boppart, S. A. Optical coherence tomography: a review of clinical development from bench to bedside. *J Biomed Opt* 12, 051403 (2007).
- Boppart, S. A., Luo, W., Marks, D. L., Singletary, K. W. Optical coherence tomography: feasibility for basic research and image-guided surgery of breast cancer. *Breast Cancer Res Treat* 84, 85-97 (2004).
- Nguyen, F. T., Zysk, A. M., Chaney, E. J., Kotyneck, J. G., Oliphant, U. J., Bellafiore, F. J., Rowland, K. M., Johnson, P. A., Boppart, S. A. Intraoperative microscopic assessment of tumor margins during breast conserving surgery using optical coherence tomography. *Cancer Research*, in press (2009).
- Luo, W., Nguyen, F. T., Zysk, A. M., Ralston, T. S., Brockenbrough, J., Marks, D. L., Oldenburg, A. L., Boppart, S. A. Optical biopsy of lymph node morphology using optical coherence tomography. *Technol Cancer Res Treat* 4, 539-548 (2005).
- Boppart, S. A., Zysk, A. M., Nguyen, F. T., Chaney, E. J., Bellafiore, F. J., Kotyneck, J. G., Johnson, P. A., Rowland, K. M. Real-time optical biopsy and analysis of breast cancer using clinical optical coherence tomography. *J Clin Onc, Proceedings of the 43rd ASCO Annual Meeting* 25, 567s (2007).
- Hsiung, P. L., Phatak, D. R., Chen, Y., Aguirre, A. D., Fujimoto, J. G., Connolly, J. L. Benign and malignant lesions in the human breast depicted with ultrahigh resolution and three-dimensional optical coherence tomography. *Radiology* 244, 865-874 (2007).

24. Zysk, A. M., Boppart, S. A. Computational methods for analysis of human breast tumor tissue in optical coherence tomography images. *J Biomed Opt* 11, 054015 (2006).
25. Iftimia, N. V., Bouma, B. E., Pitman, M. B. A portable, low coherence interferometry based instrument for fine needle aspiration biopsy guidance. *Rev Sci Instrum* 76, 064301 (2005).
26. Faber, D. J., Aalders, M. C. G., Mik, E. G., Hooper, B. A., van Gemert, M. J. C., van Leeuwen, T. G. Oxygen saturation-dependent absorption and scattering of blood. *Phys Rev Lett* 2004(93), 028102 (2004).
27. Zysk, A. M., Chaney, E. J., Boppart, S. A. Refractive index of carcinogen-induced rat mammary tumours. *Phys Med Biol* 51, 2165-2177 (2006).
28. Liang, X., Zhang, Q., Li, C., Grobmyer, S. R., Fajardo, L. L., Jiang, H. Phase-contrast diffuse optical tomography. *Acad Radiol* 15, 859-866 (2008).
29. Zysk, A. M., Marks, D. L., Liu, D. Y., Boppart, S. A. Needle-based reflection refractometry of scattering samples using coherence-gated detection. *Opt Express* 15, 4787-4794 (2007).
30. Reiser, S. J., Anbar, M. *The Machine at the Bedside*. Cambridge University Press, New York (1984).
31. Berg, W. A., Gutierrez, L., NessAiver, M. S., Bradford Carter, W., Bhargavan, M., Lewis, R. S., Ioffe, O. B. Diagnostic accuracy of mammography, clinical examination, US, and MR imaging in preoperative assessment of breast cancer. *Radiology* 233, 830-849 (2004).

*Received: April 29, 2009; Revised: August 19, 2009;*

*Accepted: August 24, 2009*

